

Table 1. Data for *Ovis*, *Capra* and *Cervus* samples from Zawi Chemi Shanidar and Shanidar Cave. Layer B1, proto-Neolithic; layer C, Baradostian; layer D, Mousterian.

Animal	Specimens (N)	Sample (%)	Metapodials (N)	Immature animals (%)
<i>Zawi Chemi Shanidar; 0.50 to 1.00 in depth</i>				
<i>Ovis</i>	63	81.0	48	54.2
<i>Capra</i>	8	10.1	8	25.0
<i>Cervus</i>	22	8.9		
<i>Zawi Chemi Shanidar; 1.00 to 1.50 in depth</i>				
<i>Ovis</i>	473	65.9	176	44.3
<i>Capra</i>	79	9.6	72	25.0
<i>Cervus</i>	576	24.5		
<i>Zawi Chemi Shanidar; 1.50 to 2.95 in depth</i>				
<i>Ovis</i>	4 (adult)			
<i>Cervus</i>	31			
<i>Shanidar Cave; layer B1</i>				
<i>Ovis</i>	27	42.9	19	57.9
<i>Capra</i>	36	57.1	14	42.9
<i>Shanidar Cave; layer C</i>				
<i>Ovis</i>	17	38.5	12	16.7
<i>Capra</i>	27	59.5	23	21.8
<i>Cervus</i>	4	2.0		
<i>Shanidar Cave; layer D</i>				
<i>Ovis</i>	8	20.4	7	42.9
<i>Capra</i>	29	75.1	9	11.2
<i>Cervus</i>	6	4.4		

from Shotwell's analysis of several Pliocene sites in Oregon (8).

The first step was to establish the number of diagnostic elements in the skeleton of each species. For sheep and goats there are 22 elements: 8 third phalanges, 8 first phalanges, 2 metatarsals, 2 metacarpals, and 2 scapulae. For the red deer there are 72: all the elements of the postcranial skeleton except the vertebrae.

Secondly, the number of specimens for each species was determined—that is, the number of identifiable bone fragments from each species in the sample.

Thirdly, the relative frequency, *f*, of occurrence of each species was calculated as follows:

$$f = \frac{\text{No. of specimens}}{\text{No. of diagnostic elements}}$$

The relative frequencies are ratios and may be expressed in percentiles. The percentage of adult and immature animals (the "immature" are those less than 1 year old) was calculated for the *Ovis* and *Capra* samples (9) (such a calculation cannot be made for the *Cervus* material until the rate of fusion of the epiphyses is better known). The results are given in Table 1.

It is evident that the economy at Zawi Chemi Shanidar was quite different from that of the Baradostian

and Mousterian levels in Shanidar Cave. Most notable is the increase in *Ovis* and *Cervus* and, in the upper levels, almost complete reliance on *Ovis* (the change is not so evident in the contemporary levels in the cave, but at present the data from these levels cannot be evaluated, since there has been considerable admixture from the historic levels). Shanidar Cave is located on a spur of the Baradost Mountains, 300 m above Zawi Chemi Shanidar on the valley floor, and it could be argued that the change represents a regional difference. Certainly, red deer would have been more common in the scrub oak forest on the valley floor than in the heights close to the cave. The shift to a high percentage of *Ovis* does not represent a regional difference, however. If sheep had been present in the valley they would have been more frequently killed as game than the goats on the heights above the cave. It is doubtful that wild sheep were ever very common in the immediate vicinity of the two sites; this is suggested by their relative scarcity in the Baradostian and Mousterian levels. The valley of the Greater Zab river at Shanidar is flat and narrow, with precipitous cliffs on each side. There is still a considerable remnant of scrub oak forest, despite the fact that it has been trimmed for fuel for centuries. The highest reaches of the mountains flanking the valley are typical of the habitat preferred by goats, and *Capra hircus aegagrus* is still fairly common in the vicinity of Shanidar. On the other hand, sheep prefer broad high pastures and the treeless grassy slopes of mountains. The results suggest that the two shifts that indicate cultural control did take place at Zawi Chemi Shanidar: (i) there is evidence of an increased reliance on *Ovis*, particularly in the upper levels of Zawi Chemi Shanidar, and (ii) the percentage of immature *Ovis* increased to approximately 50 percent. Presumably domestic sheep, morphologically identical to their wild ancestors, were introduced from some other region. Domestication of a species prior to the onset of osteological change has long been postulated by archeologists, but the data from Zawi Chemi Shanidar and Shanidar Cave are the first direct evidence of this important stage in the beginnings of animal husbandry.

DEXTER PERKINS, JR.  
Harvard, Massachusetts

#### References and Notes

1. For a description of the two sites, see R. S. Solecki, *Science* **139**, 179 (1963).
2. C. A. Reed reported the presence of domestic goats at Jarmo [*Science* **130**, 1629 (1959)]. The approximate date is 6750 B.C. [R. J. Braidwood and B. Howe, *Studies in Ancient Oriental Civilization*, No. 31 (Univ. of Chicago Press, Chicago, 1960), p. 160].
3. There are several references, notably J. W. Amschler, *Archeologia Austriaca* **3**, 26 (1949); V. Gromova, *Komissia po Izucheniiu Chetvertichnogo Perioda* **10**, 1 (1953); and M. Hildebrand, *Calif. Fish Game* **41**, 327 (1955). I was forced to discard many of the diagnostic characters proposed by these authors. My study was based on a far larger sample than theirs—one that included specimens of both wild and domestic animals.
4. C. A. Reed, in R. J. Braidwood *et al.*, *Studies in Ancient Oriental Civilization*, No. 31 (Univ. of Chicago Press, Chicago, 1960).
5. D. Perkins, Jr., *Sumer* **16**, 77 (1960).
6. H. E. Wright, Jr., in R. J. Braidwood *et al.*, *Studies in Ancient Oriental Civilization*, No. 31 (Univ. of Chicago Press, Chicago, 1960), p. 90.
7. R. H. Dyson, Jr., *Am. Anthropologist* **55**, 661 (1953).
8. J. A. Shotwell, *Ecology* **36**, 327 (1955); **39**, 271 (1958).
9. The metapodial epiphyses, which fuse at 12 to 15 months, were used to determine the percentage of young animals. The first and third phalanges, which fuse well within the first year, cannot be used, since the separate epiphyses are rarely preserved and the diaphysis alone is unrecognizable. For the epiphysal-union pattern see T. W. Todd and A. W. Todd, *Am. J. Anat.* **63**, 1 (1938), and R. N. Smith, *Vet. Rec.* **68**, 257 (1956).

23 March 1964

#### Neutron and Proton Dosages in the Upper Atmosphere from Solar Flare Radiation

Abstract. *The radiation dosage from secondary neutrons as well as from primary and secondary protons in the earth's atmosphere during solar particle events is calculated as a function of the solar proton flux, atmospheric depth, and geomagnetic-cutoff rigidity. The dosage in rems from secondary neutrons exceeds the dosage from protons below 30 g/cm<sup>2</sup> of residual atmosphere. Neutron dosages in rads are less than the dosage from primary protons at all depths above 100 g/cm<sup>2</sup>. The maximum neutron dose to travelers in supersonic aircraft during solar particle events of the magnitude observed during the last solar cycle would be of the order of 1 rem.*

Freier and Webber (1) have discussed the hazard to space travelers from solar particle beams exhibiting the two-parameter exponential-rigidity spectrum typical of such radiation. They calculate the dosage from the primary protons as a function of the two parameters and of shielding thickness from 1 to 10 g/cm<sup>2</sup>. Over this range of thicknesses, the dosage from secondary neutrons and protons produced in the

shielding appears to be small compared to the dosage from primaries. The equilibrium neutron flux, however, reaches a maximum at shielding thicknesses greater than 10 g/cm<sup>2</sup> and then falls off much more slowly with shielding thickness than the proton flux, owing to the greater mean free path of the neutrons. This was shown quantitatively in previous calculations of the equilibrium neutron flux produced in the atmosphere by solar protons (2). Hence at greater shielding thicknesses the main radiation hazard may be from neutrons rather than protons, and a judicious choice of shielding material may provide greater safety than a further increase in thickness.

In this report, we calculate the dosage in rads and in rems from the equilibrium neutron flux produced by solar protons at atmospheric depths of 1 to 100 g/cm<sup>2</sup>. These dosages are compared with the dosages from primary and secondary protons. We find that the neutron dosage exceeds the proton dosage at the altitude at which supersonic transports cruise. The neutron dosage to travelers in such aircraft during the peak of solar particle events of the magnitude observed during the last solar cycle is below the maximum permissible dosage for occasional exposure. This conclusion, however, depends on present estimates of three quantities—the intensity of solar particle radiation, the relative biological effectiveness of neutrons, and the maximum permissible exposure to radiation—which are subject to revision as more data become available.

The methods used to calculate the equilibrium neutron flux in the atmosphere produced by solar protons as well as the results of the calculation have been described (2). The differential-rigidity spectrum of the protons was assumed to have the form proposed by Freier and Webber (1):

$$dJ/dP = (dJ/dP)_0 \exp(-P/P_0) \quad (1)$$

where  $P_0$  is a characteristic rigidity of the protons which varies with time. Fig. 1 shows the energy spectra of the equilibrium neutrons at selected atmospheric depths, calculated for the estimated time-average values of  $P_0 = 125$  Mv and  $(dJ/dP)_0 = 1$  proton cm<sup>-2</sup> sec<sup>-1</sup> Mv<sup>-1</sup>. First-collision neutron dose rates were obtained by integrating (over energy) the product of the neutron energy spectra and the first-collision dose curve given in *NBS Handbook 63* (3). The neutron dose rate both in rads and in rems was calculated for various

values of  $P_0$  and for various geomagnetic-cut-off rigidities.

The dose rate in rads from primary protons was obtained by evaluating the expression:

$$1.6 \times 10^{-8} \int_{P_0}^{\infty} (dJ/dP) dP$$

$$\int_1^{x/R(E')} \exp\left[-\frac{x}{\mu L(E')}\right] \left[\frac{dE}{dx}(E')\right]_{\text{H}_2\text{O}} \frac{dx}{\mu} \quad (2)$$

where

$$E'(E, x, \mu) = E - \int_0^{x/\mu} \left(\frac{dE}{dx}\right)_{\text{air}} dx.$$

The factor  $1.6 \times 10^{-8}$  is the ratio of the dose in rads to the dose in Mev per gram. Other quantities in Eq. 2 are defined as follows:

- $P_0$  = the geomagnetic cutoff rigidity;
- $P$  = the magnetic rigidity of the incident proton at the top of the atmosphere ( $x = 0$ );
- $E$  = the energy of the incident proton at  $x = 0$ ;
- $dJ/dP$  = the differential rigidity spectrum of isotropic solar protons at  $x = 0$ ;
- $R(E)$  = the range in air of a proton of energy  $E$  (4);
- $L(E')$  = the attenuation length of protons of energy  $E'$  in air;
- $\mu = \cos \theta$ , where  $\theta$  is the direction relative to the normal of the incident proton at  $x = 0$ ;
- $(dE/dx)_{\text{air}}$  = the differential energy loss in Mev per gram of air by a proton of initial energy  $E$  (4);
- $[dE/dx(E')]_{\text{H}_2\text{O}}$  = the energy loss in Mev per gram of H<sub>2</sub>O (approximately equal to the energy loss in tissue) by a proton of initial energy  $E'$  (4).

The primary proton-dose rate in rems was obtained by inserting the relative biologic effectiveness (RBE) for protons (5) into the integral over  $\mu$  in Eq. 2 and re-evaluating the integral. Since the RBE is roughly unity for protons with energies greater than 15 Mev, only the contribution to the integral from terms near the upper limit was altered by inserting the RBE function.

Secondary proton-dose rates were calculated as a function of atmospheric depth with the aid of two assumptions: (i) The cross section for proton production in air was assumed to be equal to the cross section for neutron production. Hence, if energy losses due to excitation, recoil, and endothermic reactions are neglected, one-half the residual energy  $E'$  of the primary proton was assigned to secondary protons, and the mean energy of the secondaries was  $E'/2N$ , where  $N$  is the number of protons produced per interaction by a

Table 1. Proton and neutron dosages in rems, 12 to 16 November 1960.

Dose	Depth (g/cm <sup>2</sup> )		
	1 g/cm <sup>2</sup>	20 g/cm <sup>2</sup>	50 g/cm <sup>2</sup>
1900, 12 Nov. to 2300, 13 Nov.			
Proton	162.0	4.9	0.64
Neutron	2.1	2.3	1.25
0500, 15 Nov. to 0800, 16 Nov.			
Proton	58.0	1.5	0.27
Neutron	1.0	0.68	0.41

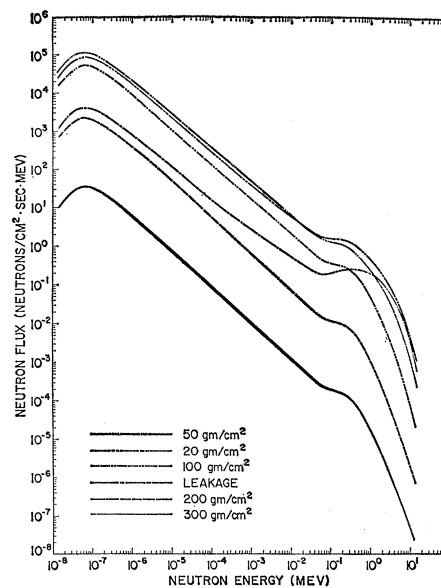


Fig. 1. Equilibrium neutron energy spectrum at various altitudes calculated for exponential proton flux spectrum  $dJ/dP = (dJ/dP)_0 \exp(-P/125\text{Mv})$ , normalized to  $(dJ/dP)_0 = 1$  proton cm<sup>-2</sup> sec<sup>-1</sup> Mv<sup>-1</sup>.

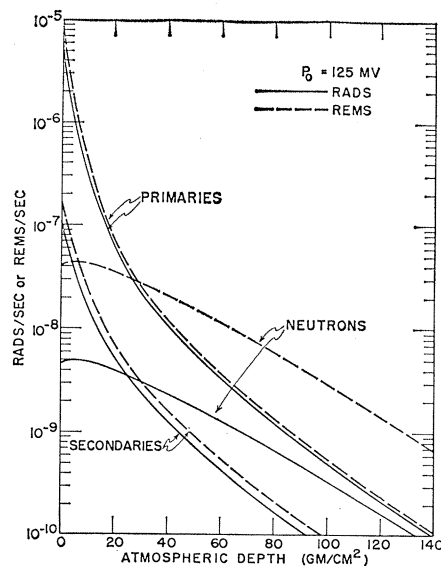


Fig. 2. Dosage from primary protons, secondary protons, and neutrons in rads and in rems as a function of atmospheric depth. The solar proton spectrum is  $dJ/dP = (dJ/dP)_0 \exp(-P/125\text{Mv})$ , normalized to  $(dJ/dP)_0 = 1$  proton cm<sup>-2</sup> sec<sup>-1</sup> Mv<sup>-1</sup>.

proton of energy  $E'$ . (ii) The secondary protons were assumed to stop within  $\mu^{-1}$  g per  $\text{cm}^2$  of their site of production. Then:

$$D(x)dx \text{ in rads} = 1.6 \times 10^{-8} \int_{P_0}^{\infty} (dJ/dP) dP$$

$$\int_1^{x/R(E')} \exp - [x/\mu L(E')][E'/2L] \frac{dx}{\mu} d\mu \quad (3a)$$

$$D(x)dx \text{ in rems} = 1.6 \times 10^{-8} \int_{P_0}^{\infty} (dJ/dP) dP$$

$$\int_1^{x/R(E')} \exp - [x/\mu L(E')] \left[ \frac{E'}{2L} + NQ \right] \frac{dx}{\mu} d\mu \quad (3b)$$

where  $(1/L)$  is the total reaction cross-section of protons of energy  $E'$ , and  $Q$  is the difference between the dose in rems and the dose in rads delivered by a proton of energy  $E'/2N$ :

$$Q = \int_{E'/2N}^0 \left[ \text{RBE}(E') - 1 \right] \left[ \frac{dE}{dx}(E') \right]_{\text{H}_2\text{O}} dE'$$

All other quantities in Eq. 3 are as defined in Eq. 2.

The neutron and proton dosages in rads and in rems, normalized to a value of  $(dJ/dP)_0 = 1 \text{ proton cm}^{-2} \text{ sec}^{-1} \text{ Mv}^{-1}$ , are shown in Figs. 2, 3, 4, and 6. It should be noted that this is approximately the time-average value of  $(dJ/dP)_0$  over the last ten solar cycles (6).

During a major solar particle event,  $(dJ/dP)_0$  may be as high as a few hundred protons  $\text{cm}^{-2} \text{ sec}^{-1} \text{ Mv}^{-1}$  for an hour or longer and may exceed  $10^7$  protons  $\text{cm}^{-2} \text{ Mv}^{-1}$  over the period of the event, generally 1 or 2 days (1). The ordinate in Fig. 2 thus should be multiplied by five or six orders of magnitude and the ordinate in Figs. 3, 4, and 6 by two orders of magnitude to obtain the dose rates in rads or rems per hour during the peak of a major solar particle event.

In Fig. 2, the neutron dosage in rads and in rems as a function of atmospheric depth is compared with the dosage from primary and secondary protons for  $P_0 = 125 \text{ Mv}$  and a cutoff rigidity of 0 Mv. The secondary proton dose increases slightly by comparison with the primary proton dose with increasing atmospheric depth but remains less than 20 percent of the primary dose at all depths up to 100 g/cm<sup>2</sup>. The primary proton dose in rems is about 10 percent larger than the corresponding dose in rads, and the secondary proton dose is 20 to 40 percent larger in rems than in rads. The neutron dose, on the other hand, is almost an order of magnitude greater in rems than in rads. This reflects the high RBE of neutrons (3) in the region below a few Mev where almost all the equilibrium neutron flux is concentrated. The proton flux at any depth

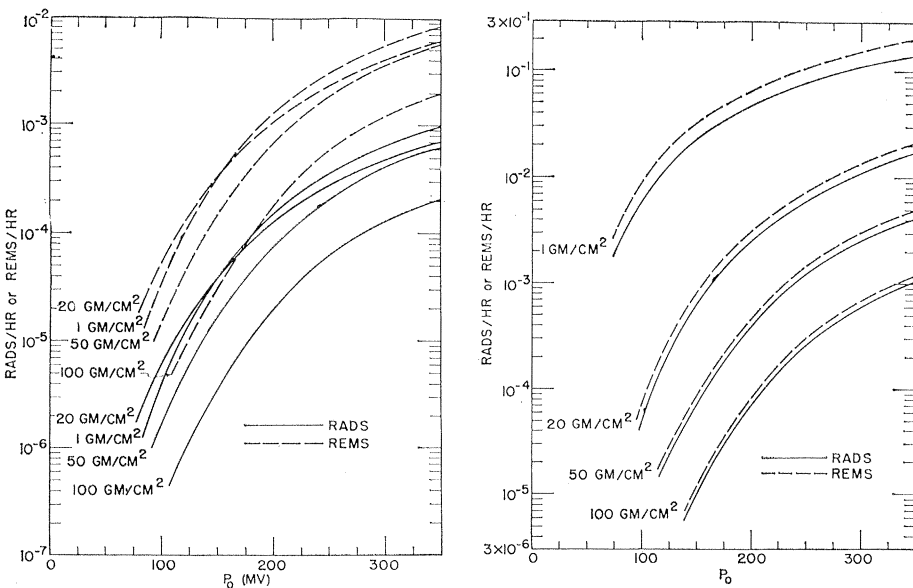


Fig. 3 (left). Neutron dosage in rads and in rems at selected atmospheric depths shown as a function of  $P_0$ . The flux is normalized to  $(dJ/dP)_0 = 1 \text{ proton cm}^{-2} \text{ sec}^{-1} \text{ Mv}^{-1}$ . Fig. 4 (right). Total (primary plus secondary) proton dosage in rads and in rems at selected atmospheric depths as a function of  $P_0$ . Flux is normalized to  $(dJ/dP)_0 = 1 \text{ proton cm}^{-2} \text{ sec}^{-1} \text{ Mv}^{-1}$ .

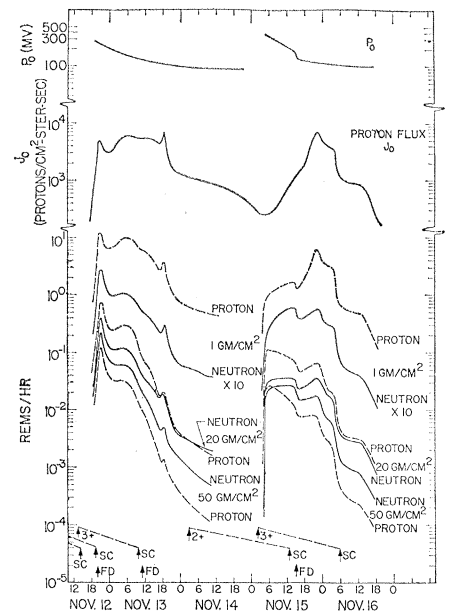


Fig. 5. Time variation of  $P_0$ ,  $J_0$  and the radiation dosage at selected atmospheric depths during the period of 12 to 16 November 1960. Solar flares (3+, 2+), Forbush decreases (FD), and sudden commencements (SC) indicated by arrows at bottom of figure.

has an average energy many times greater than that of the neutron flux and hence a much smaller average RBE. As a consequence of this difference in RBE, the neutron dose in rems exceeds the proton dose at depths greater than about 30 g/cm<sup>2</sup> (24,000 m, or 80,000 ft) (7) whereas the neutron dose in rads is less than the proton dose at all depths up to 140 g/cm<sup>2</sup>.

It should be noted that the dosages given in Fig. 2 refer to the upper surface of a body lying parallel to the top of the atmosphere under a specified thickness of air ( $x$  g/cm<sup>2</sup>). At any tissue depth  $d$  within the body, the ratio of neutron to proton dose is roughly equal to the ratio shown in Fig. 2 for an atmosphere depth of  $(x + d)$ . For example, a man lying in a supersonic aircraft shielded by 1 g/cm<sup>2</sup> of aluminum and flying over the poles at 28,500 m (19 g/cm<sup>2</sup> of residual atmosphere) (7) would receive approximately equal neutron and proton dosages in rems at the center of the body (about 10 g/cm<sup>2</sup> below the surface). At the upper body surface, in contrast, the proton dose would be more than twice the neutron dose. In general, an increase in the ratio of neutron to proton dosage toward the center of the body as compared with the sur-

face may be expected, owing to the relative flatness of curve for the neutron dose versus depth.

As pointed out by Wilson and Miller (8), the ratio of primary to secondary dose is greatly influenced by shield-target geometry and may therefore be quite different for space capsules than for a body within the atmosphere. Nevertheless, a rough estimate of the neutron dosage inside an aluminum-shielded space capsule during a solar particle event may be made from Figs. 2 through 5. The cross-section for neutron production in aluminum is approximately a factor of 1.7 times larger than the corresponding cross-section in air. If similar neutron scattering and absorption cross-sections in the two materials and similar geometry are assumed, the neutron dosage under a given thickness of aluminum shielding would then be roughly 1.7 times greater than the neutron dosage under the same thickness of atmosphere.

The proton dosage, on the other hand, is nearly independent of the composition of the shielding material over the range of elements from nitrogen to aluminum. Hence, the ratio of neutron to proton dosage would be higher under an aluminum shield than under an air shield with the same thickness and geometry.

The neutron and total proton dosages in rads and in rems at selected atmo-

spheric depths are shown as a function of  $P_0$  in Figures 3 and 4. With the aid of these curves, the total dose rate can be calculated as a function of time for any solar proton event for which the time variations of  $P_0$  and  $(dJ/dP)_0$  are known. This is illustrated in Fig. 5, which shows the time variations of  $P_0$  and  $J_0$ , where  $J_0 = P_0(dJ/dP)_0$ , 12 to 16 November 1960 (1), together with the corresponding neutron and total proton dose rates at atmospheric depths of 1, 20, and 50 g/cm<sup>2</sup>. Two 3+ solar flares occurred during the period in question, one at 1329 UT on 12 November and the second at 0221 UT on 15 November. Time-integrated dosages associated with each of the two flares are given in Table 1. The time-integrated neutron dosage exceeds the total proton dosage below atmospheric depths of 25 to 30 g/cm<sup>2</sup>.

The variation of neutron dose rate with geomagnetic cutoff rigidity is shown in Fig. 6. The decrease in proton dosage with increasing cutoff rigidity occurs predominantly at high altitudes, whereas the decrease in neutron dosage is relatively evenly distributed over all atmospheric depths. Thus, the ratio of neutron to proton dose increases at high altitudes as the cutoff rigidity is raised. This is of interest in connection with shielding of high-altitude aircraft at low latitudes and of orbiting vehicles within the geomagnetic field.

In summary, the dosage from secondary neutrons produced by solar protons exceeds the dosage from primary and secondary protons at atmospheric depths greater than 30 g/cm<sup>2</sup>. This is roughly the upper boundary at which projected supersonic aircraft can cruise (9). The neutron dosage falls by a factor of two between 30 and 50 g/cm<sup>2</sup> (between 24,000 and 21,000 meters) whereas the proton dosage falls by a factor of five over the same altitude range. Surface neutron dosages to persons flying a polar route at 24,000 meters during a major solar-particle event are of the order of 0.1 rem per hour at the peak of the event and 1 rem over the duration of the event. Such events occur about once a year during solar maximum.

Hence, the accumulated dose to pilots of supersonic aircraft appears to be below the maximum permissible level of 5 rems per year for chronic exposure (3). Further reduction of the total dosage can be accom-

plished most efficiently by shielding with materials having a high cross section for neutron absorption.

E. J. FLAMM

R. E. LINGENFELTER

*Institute of Geophysics and Planetary Physics, University of California, Los Angeles*

#### References and Notes

1. P. Freier and W. R. Webber, *Science* **142**, 1587 (1963); *J. Geophys. Res.* **68**, 1605 (1963).
2. R. E. Lingenfelter and E. J. Flamm, *J. Atmos. Sci.*, in press; *J. Geophys. Res.*, in press.
3. Natl. Bur. Std. (U.S.) Handbook 63, (1957).
4. M. Rich and R. Madey, *UCRL-2301*, Lawrence Radiation Laboratory, Berkeley, Calif. (March 1954).
5. S. J. Lindenbaum, *Ann. Rev. Nuclear Sci.* **11**, 213 (1961).
6. W. R. Webber and P. Freier, *TID-7652*, Book I, U.S. Atomic Energy Commission (1962).
7. H. Kallman-Bill, Ed., *Cospar International Reference Atmosphere*, 1961, (North-Holland, Amsterdam, 1961).
8. R. K. Wilson and R. A. Miller, *TID-7652*, Book II, U.S. Atomic Energy Commission (1962).
9. H. J. Schaefer, *Aerospace Med.* **34**, 1 (1963).
10. Publication No. 364, Institute of Geophysics and Planetary Physics, University of California, Los Angeles.

24 April 1964

#### Calcite-Aragonite Equilibrium at 100°C

**Abstract.** *The equilibrium pressure of the calcite-aragonite transition has been determined near 100°C and is 4.35 kilobars. These data are in agreement with earlier work but conflict with the most recent determination by Simmons and Bell.*

At low temperatures, the free energy of the calcite-aragonite transition is small [250 cal/mole, Latimer (1)] and direct experiments are necessary to fix the transition pressure with any degree of certainty. The low temperature data of Jamieson (2) and extrapolation of MacDonald's (3) and Clark's (4) data indicate a transition pressure of about 4.5 kb at 100°C. At low temperature, direct study is difficult because of the sluggish nature of the transition; but Dachille and Roy (5) and Simmons and Bell (6) were able to effect transitions in the range 25° to 100°C by using the oscillating squeezer. Dachille and Roy found the transition near 4 kb at 100°C. Simmons and Bell report the much higher value of 7 kb. In view of these discrepancies and the problems associated with the squeezer devices we

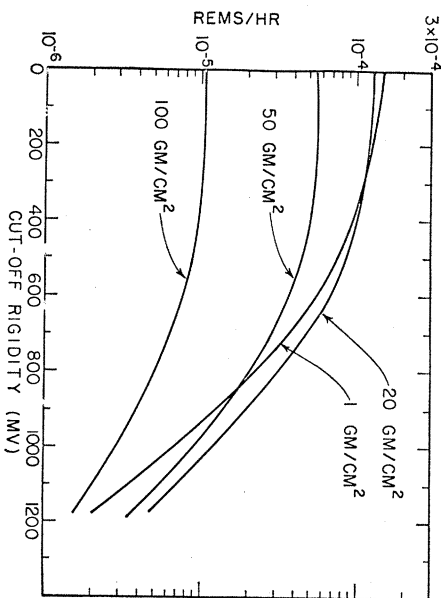


Fig. 6. Total neutron dosage in rads as a function of geomagnetic-cutoff rigidity. The solar proton spectrum  $dJ/dP = (dJ/dP)_0 \exp(-P/125\text{Mv})$  normalized to  $(dJ/dP)_0 = 1 \text{ proton cm}^{-2} \text{ sec}^{-1} \text{ Mv}^{-1}$ .